European Polymer Journal 45 (2009) 1349–1358

Contents lists available at ScienceDirect

European Polymer Journal

journal homepage: www.elsevier.com/locate/europolj

Macromolecular Nanotechnology

Physical properties of ion beam treated electrospun poly(vinyl alcohol) nanofibers

Kenneth Kar Ho Wong [a], Jeffrey L. Hutter [b], Martin Zinke-Allmang [a,b], Wankei Wan [c,d,*]

[a] Department of Medical Biophysics, The University of Western Ontario, London, Ont., Canada N6A 5C1
[b] Department of Physics and Astronomy, The University of Western Ontario, London, Ont., Canada N6A 3K7
[c] Fordham Center for Biomedical Engineering, The University of Western Ontario, London, Ont., Canada N6A 5B9
[d] Department of Chemical and Biochemical Engineering, The University of Western Ontario, Thompson Engineering Building, Room 433, London, Ont., Canada N6A 5B9

ARTICLE INFO

Article history:
Received 2 October 2008
Received in revised form 30 January 2009
Accepted 3 February 2009
Available online 12 February 2009

Keywords:
Ion implantation methods
Electrospun polymer fiber
Surface morphology
Mechanical properties

ABSTRACT

We show that the mechanical properties of nano-sized electrospun poly(vinyl alcohol) fibers can be modified using broad-energy ion beam implantation. The elastic moduli were determined using atomic force microscopy multi-point mechanical bending tests on individual fibers before and after treatment. With a dose of 8.0×10^{15} ions/cm^2 of nitrogen ion we observed 30% increases in fiber elastic modulus with a simultaneous fiber diameter reduction. Two additional doses of nitrogen ion as well as a 8.0×10^{15} ions/cm^2 of helium ion treatment showed that this stiffness improvement effect was dependent on ion dosage and ion species. The surface morphological features of the fiber mat were shown to be unaltered due to the ion beam treatment. Key chemical modifications via nitrogen ion treatment were the introduction of the functional groups amine and amide. These groups are important in promoting cell compatibility on polymer surfaces.

1. Introduction

Electrospinning [1] is a simple but versatile technique capable of producing three-dimensional non-woven fiber mats from a wide variety of synthetic and natural polymers [2] including proteins [3] for applications such as membranes [4], wound dressings [5], scaffold for tissue engineering [6] and protective clothing [7]. Electrospun fiber mats, consisting of nanometer sized fibers within a narrow range of fiber diameters, can provide exceptional performance and efficiency in these applications due to their high surface-to-volume ratios and interconnecting porous network. Of particular interest is the development of scaffolds for tissue engineering. The electrospinning technique is fast becoming the method of choice for their fabrication [8]. In addition, polymer-nanofiber scaffolds can be electrospun with controlled alignment to mimic the natural extracellular matrix [9].

Ion implantation is a well-established technique in the materials post-processing industry, largely because of its controllability and reproducibility. Choosing implantation parameters such as ion species, energy, current and dose allow us to selectively modify tribological [10], chemical [11] and physical properties [12] of a material. For temperature-sensitive polymers, the ability to control these treatment parameters becomes more critical as excessive energy deposition at the surface could cause permanent damage to the material [13,14]. Broad-energy (non-monochromatic) ion beam implantation is often used because, relative to monochromatic beam, it provides a wider range of ion doping depths, thus distributing energy over a greater depth range and minimizing thermal damage [15]. This

* Corresponding author. Address: Department of Chemical and Biochemical Engineering, The University of Western Ontario, Thompson Engineering Building, Room 433, London, Ont., Canada N6A 5B9. Fax: +1 519 8502308.
E-mail address: wkwan@eng.uwo.ca (W. Wan).

0014-3057/$ - see front matter © 2009 Elsevier Ltd. All rights reserved.
doi:10.1016/j.eurpolymj.2009.02.002

approach is commonly used for improving surface mechanical properties of bulk polymer materials (e.g., for surface hardening [16–18]). For a tissue engineered scaffold, the ability to tailor its stiffness to mimic the natural environment can induce more normal and stable cell adhesion [19,20]. For instance, implantation of helium ions results in drastic alteration of the cell adhesion properties of polypropylene and polytetrafluoroethylene [21]. Incorporating nitrogen via ion beam implantation near the surface of certain synthetic polymer scaffolds can form particular nitrogen-containing functional groups that enhance the attachment of protein and cell [22,23]. Therefore, ion beam treatment can be a convenient method to tailor both the mechanical and chemical properties of polymer surfaces for specific applications. Of particular interest is the potential ability of implanting specific ion species, nitrogen and helium, both of which have been proven to alter cell adhesion properties, to also modify the mechanical properties of polymer fibers.

The purpose of this work is to demonstrate the potential of surface ion beam treatment to modify the mechanical and chemical properties of polymer fibers prepared using electrospinning techniques. A hydrophilic poly(vinyl alcohol) (PVA) polymer is used here because of its good thermal stability, chemical resistance, biocompatibility [24]. Mechanical properties of individual PVA fibers prior to, and following, ion beam treatment were determined using an atomic force microscopy (AFM) multi-point bending test and analysis routine developed in our laboratory [25].

2. Experimental methods

2.1. PVA fiber production by electrospinning

An electrospinning solution was prepared by dissolving 10.8 wt% of PVA (molecular weight (M_w) = 89,000–98,000 g/mol, 99+% hydrolyzed, Sigma–Aldrich) in a solvent consisting of 80% de-ionized water and 20% ethanol. The solution was heated to 50 °C prior to electrospinning. Process parameters used were an electric field gradient of 1.5 kV/cm and solution feed rate of 0.18 ml/h.

For the study of fiber morphology, chemical properties and crystallinity, PVA fibers were collected on an aluminum foil in the form of a randomly orientated non-woven mat. To collect individual, isolated electrospun fibers for AFM mechanical testing, a transmission electron microscopy (TEM) grid (Structure Probe, Inc.) with 7.5 μm square mesh was used on a silicon substrate and mounted at the center of the collector.

2.2. Ion beam treatment

Nitrogen (N^+) and helium (He^+) ion beams were generated using the 1.7 MV tandetron accelerator at The University of Western Ontario. Fibers on Al foil or TEM grids (with Si substrate) were mounted on the sample holder with a 1.0 μm thick tantalum (Ta) foil (Ta, 99.9% purity, Goodfellow Cambridge Ltd.) placed to intersect the ion beam 2 mm in front of the sample. The thickness of the foil was confirmed with scanning electron microscope (SEM). Ion beam treatment was performed with the sample placed vertically at room temperature in ultra-high vacuum ($\sim 10^{-8}$ torr). The beam currents of N^+ and He^+ were limited to 180 nA and 130 nA, respectively.

The simulation software package SRIM-2008 [26] provides theoretical projection of the energies, doping depth profiles and total deposited energy distribution of the two ion species in the PVA fibers after transmission through the foil. Based on the simulated results, the Ta foil reduces the initial ion energies of 1.7 MeV for N^+ and 520 keV for He^+ to a suitable broad energy range (>0–300 keV for N^+ and >0–100 keV for He^+) for implantation into the PVA fibers with nearly identical doping depth profiles, ranging from the surface to about 900 nm deep. As expected, the total amount of energy deposited into the sample is then calculated as 3.2 times higher for N^+.

The fractions of N^+ and He^+ beam that penetrate the foil and are implanted into the fibers (the total doping yield) are 48% and 53%, respectively. However, all ion implantation doses (in ions/cm^2) reported in this work are incident doses to the fibers.

2.3. Surface characterization of PVA fibers

The suspended length and diameter (suspended portion) of all fibers for AFM measurements were determined from SEM topological images, which were obtained with a Leo 1530 (LEO Electron Microscopy Ltd) at 1 or 2 kV, using the Java-based image processing program, ImageJ (National Institutes of Health). No conductive coating was applied to the samples.

X-ray diffraction (XRD) spectra were collected using a Rigaku-MiniFlex powder diffractometer with a Cu-Kα radiation source operating at 30 kV and 15 mA. The 2θ spectra were scanned from 10.0° to 70.0° with a 0.1° step size.

X-ray photoelectron spectroscopy (XPS) system from Kratos Axis Ultra was used with a 210 W Al-Kα monochrome source to analyze the chemical modifications resulting from the ion beam treatments of the fibers. The pass energy of the survey scan was 160 eV and the high-resolution scan was 20 eV. The program CasaXPS (Casa Software Ltd.) was used to construct and curve-fit multiple peaks for the data envelop that appeared in the core-level energy spectra based on the built-in Marquardt–Levenberg [27] optimization algorithm.

2.4. Nanomechanical measurements using the AFM

Mechanical testing of individual PVA fibers was performed using a multimode AFM with a Nanoscope IIIa controller (Veeco Instruments) at room temperature with relative humidity between 22% and 35%. Two different triangular silicon nitride cantilevers (NP Series Probes, Veeco Instruments) with nominal spring constants of 0.32 and 0.12 N/m, respectively, were chosen to carry out imaging and mechanical testing of the native unmodified and ion-beam modified fibers. The actual spring constants were determined using the thermal noise technique [28] as $k_1 = 0.21 \pm 0.01$ N/m and $k_2 = 0.097 \pm 0.002$ N/m, respectively. These values were periodically confirmed during the experiments.

Prior to mechanical testing, optical microscopic images were used identify the precise location of every suitable fiber on TEM grid. These served as a map for AFM and SEM measurements before and after ion beam treatment. Contact AFM images of the targeted area were used to adjust the scanning position and size to include the entire suspended portion and a sufficient fraction of the supported portion on both ends of each target fiber with a minimal scan size.

Several approaches of AFM-based measurement of mechanical properties of individual fibers have been developed [29,30], but performing a bending test on the suspended section of a clamped fiber in the AFM force–volume mode, as described previously [25], allows the fiber to be examined before and after ion beam treatment. The force spectra with the z-scan size limited at 500 nm were acquired for positions in an array of 64 × 64 pixels spanning square regions of width 3.5–5.0 μm at a z-scan rate of 5 Hz. Another 64 × 64 pixels topographical image is acquired simultaneously by recording the piezo height required to achieve the trigger threshold corresponding to the maximum force; the maximum force applied to the sample was 37 and 17 nN for the stiffer and softer cantilevers.

We chose 27 fibers with diameters in the range of 106–155 nm and suspended lengths of 3.1–5.6 μm on two separated TEM grids for AFM mechanical testing to investigate the effect of N^+ and He^+ treatment. A representative example of such a fiber is shown in the SEM image of Fig. 1a. This range of fiber size allowed all mechanical measurements to be conducted with a single AFM tip under fixed operating parameters in the force–volume mode. The diameter D of the fiber was determined from a higher resolution SEM image on the suspended portion of the fiber, as shown in the inset of Fig. 1a. We averaged the diameter of 10 locations along the fiber axis. For the fiber shown, the average diameter was 114 ± 4 nm, where a standard derivation of ±4 nm was due the diameter irregularity of the electrospun fiber.

The clamped-beam model was applied to analyze the experimental data. A suspended fiber of length L is

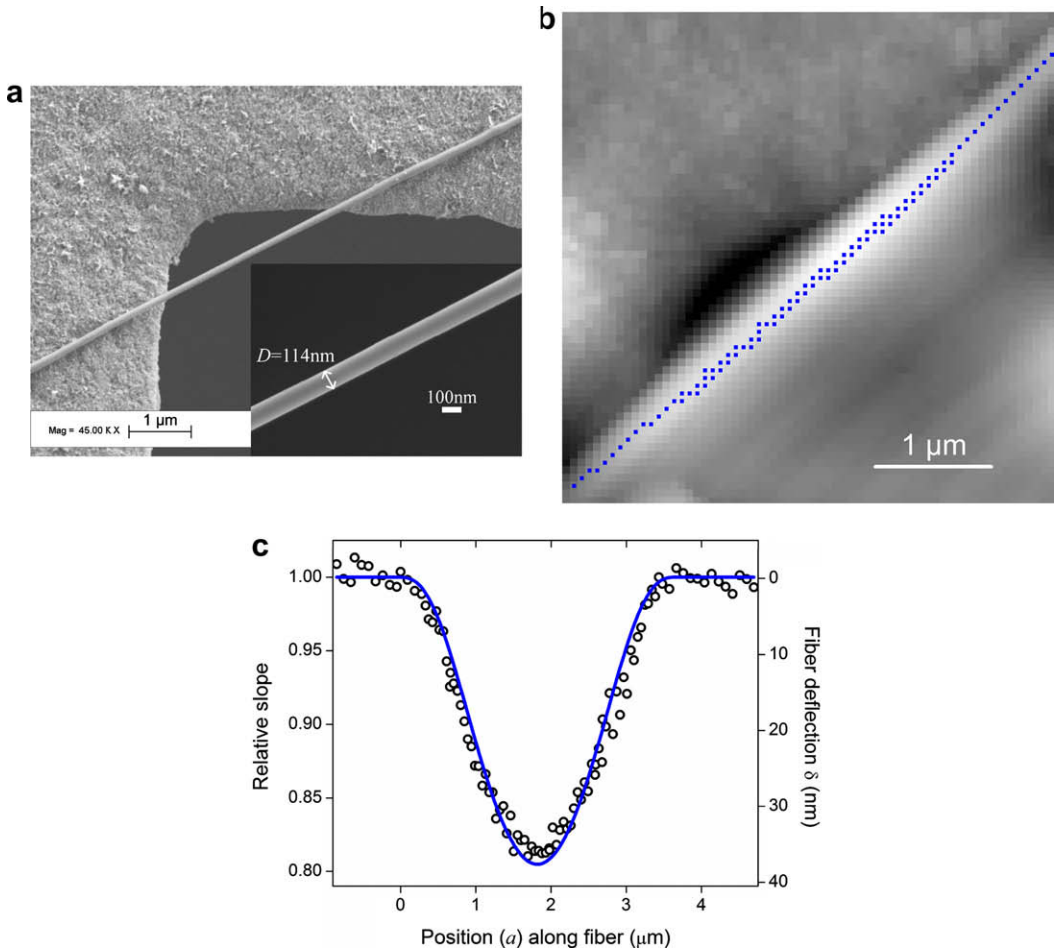

Fig. 1. (a) SEM image of a fiber suspended across a corner of a TEM grid hole. The inset at the lower right shows a high resolution SEM image of the same fiber measuring an average diameter of 114 nm. (b) A topographic image from the AFM force–volume measurement with 92 data points chosen along the fiber. (c) Plot of the slopes of force spectra (hollow circles) as a function of position a along a suspended fiber of length L = 3.7 μm. The best-fit using the clamped-beam model is shown as a solid curve.

subjected to an applied force F caused by an AFM tip, which is applied at a distance a from one of its ends. The deflection $\delta(a)$ of the fiber due to tensile deformation follows [31]:

$$\delta(a) = \frac{F}{3EI}\left[\frac{a(L-a)}{L}\right]^3 \quad (1)$$

where E is Young's modulus of the fiber and I is its area moment of inertia.

The force curve is varying with the sample displacement (Δz), which in turn equals to the sum of the cantilever deflection (Δy) and the fiber deflection ($\delta(a)$) in the contact regime. The force applied by the AFM cantilever is given by $F = k\Delta y$, where k is the spring constant of the cantilever. The slope of the position along a suspended fiber is predicted as:

$$\frac{dy}{dz} = \left[1 + \frac{k}{3EI}\left(\frac{a(L-a)}{L}\right)^3\right]^{-1} \quad (2)$$

The only variable on the right side of Eq. (2) is Young's modulus of the fiber. E is determined by fitting this equation to the (normalized) slopes measured as a function of position a along the fiber using the Levenberg–Marquardt [32] nonlinear least-squares fitting algorithm.

Data was extracted from the force–volume images and analyzed using the Igor Pro software package (Wavemetrics) with a custom analysis routine. The elastic modulus was determined from fits to the data of typically more than 60 force spectra chosen from suspended and supported sections along the fiber in a given force–volume image. To select the data points, a topographic image was used to identify the midline of the fiber, as illustrated in Fig. 1b with 92 data points (this image shows the same fiber as Fig. 1a). Generally 2 points were selected close to the midline along every row of pixels crossing the suspended portion of the fiber. Note that only 1 point was selected on the supported portion, as these points do not enter into the curve-fit and are only used to validate the calibration of the deflection sensitivity.

The slopes of the chosen force spectra and the relative fiber deflections were plotted as a function of position a from one end of the fiber, as shown in Fig. 1c. The solid line in the figure is a fit to Eq. (2). The agreement between experimental data and the derived curve for a clamped-beam model provides confidence that the experimental AFM multi-point mechanical test data validates the model.

3. Results and discussions

3.1. Electrospun PVA fiber diameters

To produce polymer fibers with a particular diameter range, an appropriate set of parameters for the polymer solution and the electrospinning process had to be chosen. We used PVA with M_w range of 89,000–98,000 g/mol. This value plays a significant role in the physical properties of the polymer solution (viscosity, conductivity and surface tension), and affects the final morphology of individual fibers. The role of the M_w on the PVA fiber morphology has been studied in detail by Koski et al. [33]. They showed that medium M_w (50,000–98,000 g/mol) PVA produces bead-free fibers with circular cross-section at a relatively low solution concentration. We also heated the 10.8 wt% PVA solution to 50 °C prior to the electrospinning process; this can reduce polymer chain entanglement and viscosity, which then decreases the surface tension of the solution. Therefore, it allows us to obtain more fibers in a fixed deposition period with a smaller diameter range compared to the solution in room temperature [34].

The diameter distribution of a fiber mat was determined from 400 randomly chosen fibers on 10 SEM images captured randomly inside a 4 mm^2 area. The two fiber mats for N^+ and He^+ treatments had original mean diameters of 117 with a standard deviation of 23 nm and 95 ± 15 nm, respectively. The results are shown in the histograms along with best-fit normal distributions in Fig. 2a. One-way ANOVA test showed a significant difference ($P < 0.01$) in the fiber diameter between the two samples. We obtained these two samples using a single 10.8 wt% PVA solution under similar electrospinning conditions, but on two separate days. We attribute this to the only uncontrolled parameters, humidity. Since the PVA solution consisted of 80% of H_2O, humidity is expected to have a large impact on the evaporation rate of the solvent during the whipping motion of the polymer jet. When the solvent evaporates at a higher rate as would occur in a low humidity environment, the electric field to have less time to stretch the jet into a smaller diameter. On the other hand, high humidity can delay the solidification of polymer jet, which would extend the stretching process to produce smaller fibers. As our result shows that the difference of the fiber diameter caused by the variation of humidity is similar to the study reported by Tripatanasuwan et al. [35].

3.2. Effect of ion beam treatment on fiber diameters

We converted a high-energy mono-energetic ion beam generated from a conventional ion implanter into a low poly-energetic beam using a Ta foil as an energy diffuser. The energy of the beam is reduced and broadened through the collision/straggling process with the Ta atoms before a portion of it is transmitted out of the foil, providing a wide implantation zone [36] in a single process, which in our case covers the range from the surface to 900 nm depth (theoretical SRIM value) of a PVA fiber mat. Using a mono-energetic beam we would need multiple-energy implantation steps to achieve a similar range. Furthermore, the ion energy deposition profile has also been extended into a wider range, minimizing energy-related damage, particularly near the surface.

The high atomic mass of Ta can reduce, but not completely eliminate, the probability of recoil and/or sputtering of foil atoms to the sample. Indeed, the XPS data in later section showed that the surface of nitrogen treated PVA fiber mats contained a significant amount of Ta atoms, which could not be ignored if the treatment was for biomaterials application. However, Ta has long been used as a contrast agent in X-ray imaging and a material in orthopedic implants, and shows cell compatibility [37,38] and no systemic toxicity inside body fluids [39], the presence of

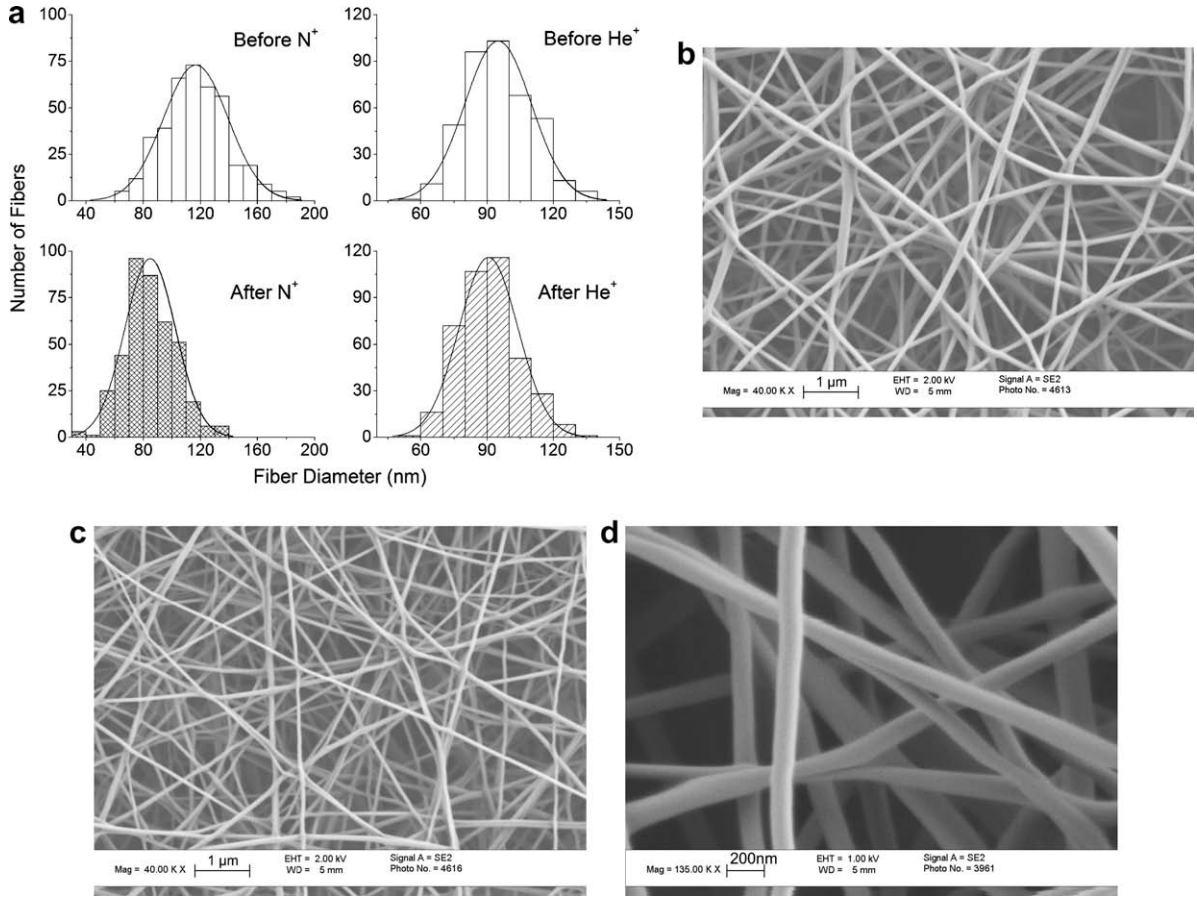

Fig. 2. (a) Histograms of the fiber diameter before and after N^+ and He^+ treatment. (b) SEM image of the original PVA fiber mat prior to ion beam treatment. (c) SEM image of the PVA fiber mat after treatment with N^+ dose of 1.2×10^{16} ions/cm^2. (d) High resolution SEM image of the PVA fibers after treatment with N^+ dose of 1.2×10^{16} ions/cm^2.

Ta is not expected to diminish the potential of applying this surface treatment technique to any suitable material for biomedical applications.

Fig. 2b shows SEM topological image of the PVA non-woven fiber mat with diameter of 117 ± 23 nm before N^+ treatment. Fig. 2c shows SEM topological image of the same fiber mat after exposure to 1.2×10^{16} ions/cm^2 of N^+. Visual comparison between Fig. 2b and c indicate that fiber diameter is reduced after ion beam treatment, which also alters the porosity and surface area to volume ratio of the mat, but the bulk porosity is expected to remain unchanged due to the relatively shallow (~900 nm) ion implantation range. Histogram of fiber diameter for the sample after N^+ treatment is shown in Fig. 2a. The treatment resulted in a significant reduction (one-way ANOVA; $P < 0.01$) in fiber diameter of 27% to 85 ± 18 nm, with a reduced diameter distribution from an original range of 63–182 to 40–140 nm. This may be attributed to an ion beam induced annealing effect [40] from the N^+ beam, the kinetic energy of the ions deposited in the fiber with a fraction converting to thermal energy. During the chain scission and cross-linking process, the thermal energy may allow the polymer chains to become mobile and re-arrange their orientations to minimize free space present in the original structure. Fig. 2d shows a high resolution SEM image of fibers with the same dose of N^+ treatment, in this image no damage to the cylindrical structure of individual fibers nor to the non-woven surface morphology of the mat is apparent.

In parallel, the second PVA non-woven fiber mat was analyzed before He^+ treatment. The surface morphology of this sample was nearly identical to that of equivalent to Fig. 2b, but diameter distribution had a slightly lower mean value of 95 ± 15 nm before ion beam exposure. After exposure to 1.2×10^{16} ions/cm^2 of He^+, no effect on the fiber diameter was observed with a final diameter of 91 ± 13 nm. With 3.2 times less energy deposited than the N^+ beam, the fibers at the surface encounter less internal annealing process and lead to no significant diameter shrinkage from the He^+ beam. The fiber diameter histogram for the sample after He^+ treatment is shown in Fig. 2a.

In contrast, our previous work, which used a monoenergetic oxygen ion beam [13], resulted in modification that was mostly destructive for polyurethane fibers. The highly localized energy deposition from a monochromatic low energy ion beam can also induce major carbonization [10,14] and melting [13] at the surface of polymeric

materials. Similar irreversible surface morphological damages are also expected from using plasma-based ion implantation systems. Although plasma-based ion implantation is frequently used to vary the original properties and/or introduce new features for particular applications [22,41–43], its high rate of destructive surface sputtering (surface erosion) does not permit treatment of polymeric materials with valuable nano-sized physical features on the surface.

3.3. N^+ treated PVA fibers and effect of ion dosage

We used the same AFM force–volume mode protocol to measure the same fibers at the same locations before and after ion beam treatment to determine its effect on the elastic moduli of individual fibers. The Young's moduli of 10 fibers were first found to have an original mean value of 30 ± 5 GPa, where the uncertainty is the standard deviation of the 10 fibers. We found good reproducibility and consistency of these results by further repeating the measurements on randomly selected fibers.

Those fibers were then exposed to 8.0×10^{15} ions/cm^2 of N^+ under the conditions (including beam current) described in Section 2.2. We lowered the dose to two-thirds of the value applied to the non-woven mat to reduce the decrease in fiber diameter we observed in previous Section 3.2. This was necessary to maintain a large enough diameter for AFM measurements using the same settings with the same cantilever.

The result from the first N^+ treatment showed an increase in elastic modulus for all 10 fibers, with the average increasing from 30 ± 5 to 39 ± 5 GPa (one-way ANOVA; significant with $P = 0.01$). The mean diameter decreased (one-way ANOVA; significant with $P < 0.01$) from 122 to 108 nm with a standard deviation of ±8 nm. Fig. 3a and b summarizes the results of mechanical testing results and the average fiber diameter of the 10 fibers, respectively. It is important to note in this context that based on our AFM contact mode images the shrinkage of the diameter did not affect the clamping condition of the fibers on the TEM grid. This was later confirmed for the rest of the ion beam treatments. Therefore, the clamped-beam model remained valid for determining the elastic modulus of the fibers from the AFM force–volume data.

The next dose step of 8.0×10^{15} ions/cm^2 of N^+ resulted in the apparent onset of a transition stage with two classes of results. For eight of the 10 fibers, we observed a further 10% increase of the elastic modulus to 43 ± 5 GPa (excluding the results of the other two). On the other hand, two fibers experienced ~36% drop from their original values. These two fibers maintained the same diameter as measured after the first treatment. If we summarize the results of all 10 fibers we find the same value as after the first treatment with a mean elastic modulus of 39 ± 11 GPa and a mean diameter of 110 ± 8 nm, the higher uncertainties in the elastic modulus due to the two deviating fibers. The modifications in elastic modulus and diameter were both significantly different (one-way ANOVA; $P < 0.01$) from the original values, but insignificantly different (one-way ANOVA; $P > 0.05$) from the values after the first treatment.

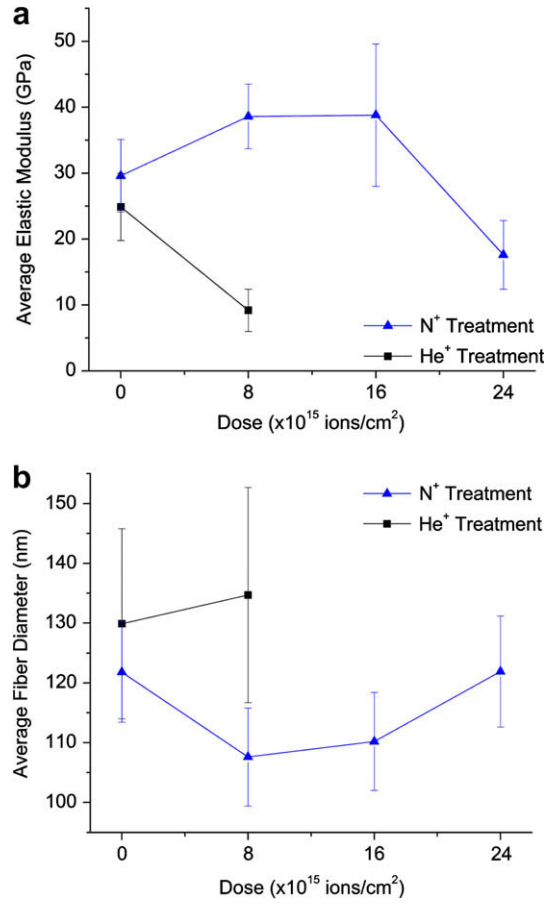

Fig. 3. (a) The average elastic modulus, and (b) the average fiber diameter of the fibers before and after each step of nitrogen ion treatments (triangle) and helium ion treatment (square).

The last step of N^+ treatment then showed the expected result for an overdosed polymer that began to carbonize. All 10 fibers showed weakening to a mean elastic modulus of 18 ± 7 GPa, which is significantly (one-way ANOVA; $P < 0.01$) 54% and 40% drop from the first two treatments and initial mean value, respectively. The mean diameter of the 10 fibers increased to a value of 122 ± 9 nm, which matches the original value.

We measured the PVA fibers with a small diameter range from 100 to 160 nm for two major reasons. First, this can minimize any variation of the elastic modulus with diameter as has been reported for polymer fibers on the nanometer scale [44,45]. Additionally, the stiffness of these fibers all fall within the operational range of a single cantilever, which allows us to perform the mechanical tests on all pre-treated (as well as all post-N^+ treated) fibers with a single set of force–volume mode parameters (such as trigger threshold and z-scan size). This avoids any need for extra calibration steps and equalizes the instrumental uncertainty for all fibers. Moreover, the small diameter range minimizes variations in the ion implantation profiles [13] that would occur for fibers of different diameters.

The results indicate that N^+ treatment results in an overall increase in stiffness of the PVA fibers up to a certain total ion dosage (1.6×10^{16} ions/cm^2). This stiffness increase can be attributed to the creation of three-dimensional cross-linked polymer chain networks (solubility results shown in Fig. 5) via ion–polymer interaction that results in chain scission, cross-linking, doping and annealing. In addition, there is an incorporation of nitrogen functionalities into the fibers (XPS results shown in Fig. 4), a change in crystallinity (Fig. 6) and a decrease in fiber diameter with a concomitant increase in density (fiber diameter results shown in Fig. 2). All these factors combined are likely led to the observed stiffness increase of the N^+ treated PVA fibers.

3.4. He^+ treated PVA fibers

Seventeen PVA fibers deposited on another TEM grid were treated with a single dose of 8.0×10^{15} ions/cm^2 of He^+. Their elastic moduli were reduced so drastically that an AFM cantilever of smaller spring constant (0.097 N/m) was required to obtain reliable force spectra after the treatment. The elastic modulus of the 17 fibers before the treatment had a mean value of 24 ± 5 GPa with a mean diameter of 130 ± 16 nm. After the He^+ treatment, the elastic modulus dropped dramatically (one-way ANOVA; $P < 0.01$) by about 63% to 9 ± 3 GPa while the diameter remained at 135 ± 18 nm; we thus did not continue helium ion beam treatment. Fig. 3a and b shows the results of the 17 fibers before and after this treatment.

3.5. Effect of ion beam treatment on chemical structure

Chemical composition of the PVA fiber mat was analyzed using XPS. It showed the chemical composition of standard PVA [46] with 71 ± 1% carbon and 29 ± 1% oxygen in the survey spectrum. This baseline can allow us to follow the degree of carbonization induced by the broad-energy ion beam surface treatment on the fibers due to incremental ion dose steps. The first 8.0×10^{15} ions/cm^2 of N^+ increased the proportion of carbon to 79.3 ± 0.2% and decreased oxygen to 20.0 ± 0.3%. The carbonization effect continued in the same trend for the second dose step and finally reached 87.2 ± 0.5% of carbon with 10.3 ± 0.1% of oxygen after the third (last) N^+ dose step. On the other hand, despite He^+ transferring a lower amount of energy, the carbonization effect induced by the first 8.0×10^{15} ions/cm^2 of He^+ matches that for the third N^+ dose with relative concentration of 86.7 ± 0.5% and 13.3 ± 0.1% of carbon and oxygen, respectively. A second He^+ dose was applied and did not further increase the concentration of carbon significantly, which remained at 87.2 ± 0.5%.

XPS survey spectra were also used to partially confirm the simulated doping profile of the transmitted ion beam we obtained from SRIM (Section 2.2). The relative concentration of the nitrogen started at 0.45 ± 0.02% for the first nitrogen dose step and reached a maximum of 2.0 ± 0.5% for the last step. No nitrogen was found in the He^+ treated sample, as expected. As helium is undetectable in XPS measurements, the amount of helium remaining in the sample after the ion implantation process is

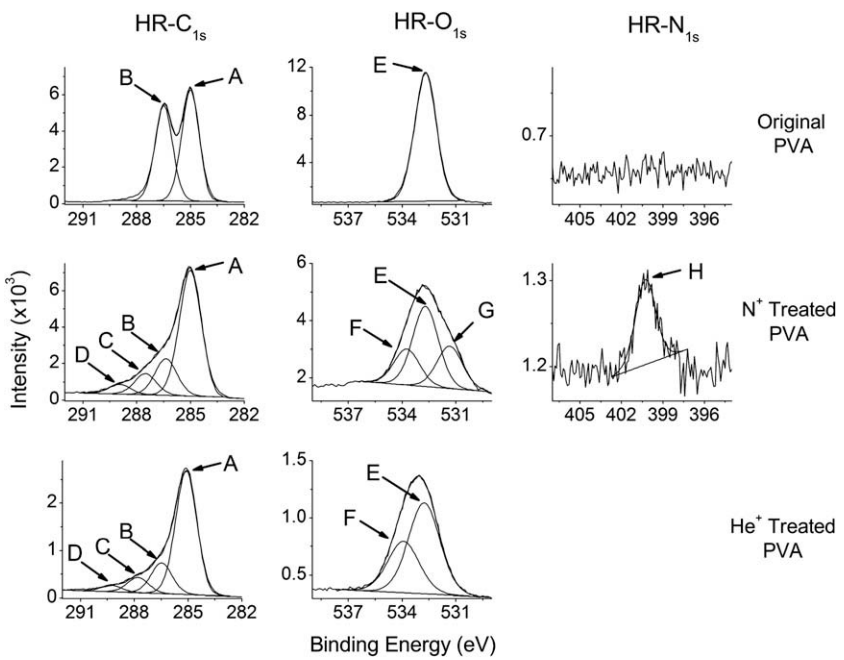

Fig. 4. High resolution XPS spectra for C_{1s} (left column), O_{1s} (middle column) and N_{1s} (right column), measure for untreated (top row), N^+ treated (middle row) and He^+ (bottom row) PVA fiber mats. The peaks are interpreted on terms of contributions from various chemical groups (lettered peaks), as defined in Table 1.

indeterminable. However, since helium is non-reactive and has a high diffusion coefficient, we expect the amount remaining in the treated sample to be negligible.

The use of Ta foil as an energy diffuser results in the incorporation of this element. XPS data confirmed the presence of Ta in all treated samples, with amounts ranging from 0.15% for the He^+ treated samples to 0.3–0.7% for the N^+ treated samples.

To test for modification of the chemical structure caused by ion implantation, high resolution (HR) XPS spectra of C_{1s}, O_{1s} and N_{1s} were obtained. Fig. 4 shows the HR XPS spectra of C_{1s} (1st column), O_{1s} (2nd column) and N_{1s} (3rd column) for the original PVA fiber mat (top row), as well as the N^+ (middle row) and He^+ (bottom row) implanted samples. The binding energy of each peak was used to determine the corresponding chemical functional groups in the sample. Every peak was labeled alphabetically as shown in Fig. 4. Table 1 provides the list of functional groups registered for each peak with the corresponding binding energy. The C_{1s} and O_{1s} spectra for the untreated PVA fiber mat matched standard PVA in the database [46]. The curve-fitted peak A and B in the C_{1s} spectrum were 53.4 ± 0.6% and 46.6 ± 0.6%, respectively. In this case, the functional group C—OH (alcohol) was the only signal to generate peak B as well as the peak E (100%) in the O_{1s} spectrum.

After N^+ treatment, the most obvious change was a new peak H (100%) created in the N_{1s} spectrum. This confirmed that implantation of the reactive ions results in chemical reactions. New groups include a reaction with carbon in PVA to form C—N groups (amine and/or amide). In the O_{1s} spectrum, two new peaks (F and G) occurred after the N^+ implantation. Peak G with a binding energy of 399.9 eV corresponds to the N—C=O (amide) group. Combining the results with the N_{1s} spectrum allows us to confirm the formation of an amide group via N^+ implantation. Furthermore, the percentage of peak G in the O_{1s} spectra increased with N^+ dose, starting from 21 ± 2% for the first dose step, increasing to 31 ± 1% after the second step, reaching 35.8 ± 0.2% for the last step. This showed a strong correlation between the trend of the relative concentration and the dose of N^+ implanted in the sample.

C_{1s} spectra evolved almost identically for N^+ and He^+ treatment with two new peaks (C and D) supplementing the two original peaks (A and B), as shown in Fig. 4. Since peak C has the same binding energy as the carbon in the amide group, the designation of peak C in the N^+ implanted sample appeared obvious. However, the observation of the same peak C for the He^+ implantation proved this peak is not exclusive to an amide group. In fact, peak C can also be due to the oxygen-containing hydrocarbon group O—C—O. This observation explains the trend of the percentage of peak C, which started at 11.1 ± 0.2% after the first N^+ dose and decreased to 4.2 ± 0.1% with the last dose. As the O_{1s} spectra shows, the number of amide groups indeed increased steadily with the N^+ dose, but the overall number of oxygen atoms dropped as the dose is increased. As more and more oxygen atoms had been recoiled away from the N^+ straggling path, the implantation process changed from creating O—C—O groups to eliminating them. Peak C has a percentage of 8.7 ± 0.1% after the first He^+ dose, and then remains at 10 ± 0.1% after the second dose.

The new peak D, with a binding energy at the high-end of the C_{1s} data envelope, belongs to the carbon in the carbonyl part of C—O—C=O (carboxylic ester) group, where the other carbon appears within peak B. Peak D shows a trend similar to that of peak C: beginning at 5.5 ± 0.2% after the first dose of N^+, then down to 3.0 ± 0.1% with the third dose. For the He^+ treated sample, the carboxylic ester group is also created at a slightly lower percentage of 3.6 ± 0.1% from the first dose, and remains at 4.6 ± 0.1% after the second dose.

Generally, the ion implantation process recoils hydrogen atoms at a rate higher than carbon and oxygen atoms from both the hydroxyl groups and the carbon backbone of the PVA molecules. We expected that C—O—C groups could be formed between two PVA chains as the cross-linker [10]. This is especially relevant to PVA as it belongs to a category of polymers favoring cross-linking [47] during the implantation process. We were not able to confirm this conclusion with our XPS data because the C—O—C binding energy overlaps with other peaks. A similar situation occurred for the C—N (amine) group with signals mixed in peaks H and B.

To confirm the introduction of cross-linking by the N^+ treatment, we conducted a solubility test on the PVA fibers pre- and post-treatment with 1.2×10^{16} ions/cm^2 of N^+. Fig. 5 shows an SEM image of the boundary area of the untreated (right side) and N^+ treated fibers (left side) after

Table 1
List of different chemical functional groups represented by the peaks labeled in XPS spectra at the corresponding binding energy shown in Fig. 4.

Peak	Functional groups	Binding energy (eV)
A	C—C*	285
B	C*—OH or C*—N or C—O—C* or C*—O—C=O	286.5
C	O—C*—O or N—C*=O	288
D	C—O—C*=O	289.1
E	C—O*H or C—O*—C or C—O—C=O*	532.7
F	O—C—O* or C—O*—C=O	533.5
G	N—C=O*	531.5
H	C—N* or N*—C=O	399.9

* is designated to the source atom in the functional group.

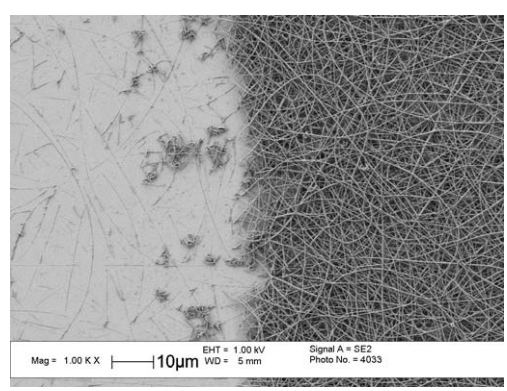

Fig. 5. SEM image of the boundary area of the original (right side) and treated fibers (left side) after 10 min of soaking in water.

10 min of soaking in water. Only minor residue of the original fibers remained on the right side but most of the fibers dissolved. It can be seen that the untreated fibers produced from an aqueous solution is stabilized by cross-linking and are stable against dissolution when exposed to water.

Chemical modifications to the polymer chains occur in parallel to physical modifications during ion beam implantation. As the ion–polymer interaction induces an irreversible chain scission and cross-linking effect into the polymer matrix, new functional groups are created as free radicals temporarily increase the chemical reactivity. With the ion beam energy broadened with a Ta foil, the doping effect start at the surface of the fiber mat. Our XPS data showed that without the presence of nitrogen, as with He^+ treatment, chemical modifications along the implantation path only generate new functional groups, such as carboxylic ester, from chain scission and cross-linking within PVA molecules. Although this has been shown to alter cell adhesion on polypropylene and polytetrafluoroethylene [21], these materials have chemical compositions very different from PVA, which generates different types of functional groups. Doping with N^+ generates amine and amide functional groups. As cell adhesion is found to improve with the introduction of such groups at the surface of polymeric materials [22,48], this N^+ treatment technique may be useful for improving cell compatibility on the treated PVA fiber surface.

3.6. Effect of ion beam treatment on crystalline structure

After He^+ and N^+ treatment, the fiber mats were analyzed by XRD techniques to determine their crystalline structure. Fig. 6 shows the XRD spectra of electrospun PVA fibers before and after various stages of the two different ion beam treatments for regions of $30° < 2\theta < 70°$. The figure also includes a comparison to PVA powder. The PVA fibers show some degree of crystalline structure relative to the PVA powder, with one weak Bragg peak (A) at $2\theta = 35°$, one medium peak (B) at 55.4° and one intense reflection peak (C) at 68.5°. The crystalline structure of the original fibers provides a baseline for studying the effect of ion beam implantation.

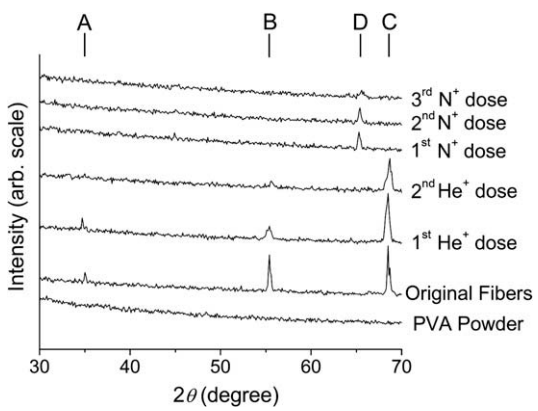

Fig. 6. XRD spectra (with four 2θ indexes at the top) of PVA powder, original electrospun PVA fiber mats, two dose steps of helium ion beam treatment and three dose steps of nitrogen ion beam treatment applied to the PVA fiber mats (offset for clarity).

The first dose of He^+ treatment showed a deterioration of the original crystalline structure at the peak (B) at 55.4° and a broadened peak (C) at 68.5°, which is consistent with the weakening of elastic modulus observed with AFM. The second dose of He^+ treatment showed a further deterioration of crystallinity (with the peak (A) at 35° disappearing along with a continued drop in intensity at the other two 2θ values). On the other hand, during N^+ treatment, the deposition energy is significantly higher than for He^+ to achieve an identical doping depth profile. As shown in Fig. 5, after the first dose of treatment the original crystalline structure of the fiber completely disappeared and a new peak (D) is seen at $2\theta = 65.4°$. This can explain the overall 30% increment on the elastic modulus of the fibers. The XRD spectrum after the second N^+ dose was almost identical. This is consistent with the results of AFM mechanical testing on the fibers, which showed no significant weakening. The last N^+ dose caused the intensity of the new peak to drop by more than 50% which is similar to the trend of average elastic modulus to decrease about 50% of the value of the first N^+ dose.

4. Conclusions

We developed simple procedures to make use of ion implantation with a broad energy range ion beam as a post-processing treatment technique to modify the elastic modulus as well as the chemical structure of electrospun PVA fibers without damaging the surface morphological features.

We confirmed that the macroscopic-scale stiffening effect occurs in nano-sized electrospun fibers, using an AFM study with multi-point mechanical bending tests performed on individual fiber before and after ion beam treatment. With a treatment of 8.0×10^{15} ions/cm^2 of N^+, we observed a 30% increase in the elastic modulus. Meanwhile, the fiber diameter decreased by up to 11%. Two additional N^+ treatments with the same dose showed that the improvement in the elastic modulus is dosage dependent. At the same time, key chemical modifications were achieved with the introduction of amine and amide functional groups using N^+ beam which could improve cell compatibility of PVA fibers. Treatment by He^+ with a dose of 8.0×10^{15} ions/cm^2, on the other hand, showed the opposite trend, with a degradation of 63% in elastic modulus and no significant change in fiber diameter.

The approach developed is generally applicable to electrospun polymer fibers for control of their mechanical properties and chemical modification for cell compatibility.

Acknowledgements

This work was supported by the Natural Sciences and Engineering Council of Canada (NSERC). We acknowledge technical assistance from Jack Hendriks, James Francis and Mark Biesinger (Surface Science Western).

References

[1] Formhals A. US Patent 2187306; 1940.
[2] Li D, Xia Y. Electrospinning of nanofibers: reinventing the wheel? Adv Mater 2004;16(14):1151–70.
[3] Li M, Mondrinos MJ, Gandhi MR, Ko FK, Weiss AS, Lelkes PI. Electrospun protein fibers as matrices for tissue engineering. Biomaterials 2005;26(39):5999–6008.
[4] Gopal R, Kaur S, Ma Z, Chan S, Ramakrishna S, Matsuura T. Electrospun nanofibrous filtration membrane. J Membr Sci 2006;281(1–2):581–6.
[5] Khil MS, Cha D-Il, Kim HY, Kim IS, Bhattarai N. Electrospun nanofibrous polyurethane membrane as wound dressing. J Biomed Mater Res 2003;67B(2):675–9.
[6] Xu CY, Inai R, Kotaki M, Ramakrishna S. Aligned biodegradable nanofibrous structure: a potential scaffold for blood vessel engineering. Biomaterials 2004;25(5):877–86.
[7] Adam D. A fine set of threads. Nature 2001;411:236.
[8] Li WJ, Cato T Laurencin, Edward J Caterson, Rocky S Tuan, Ko FK. Electrospun nanofibrous structure: a novel scaffold for tissue engineering. J Biomed Mater Res 2002;60(4):613–21.
[9] Li D, Wang Y, Xia Y. Electrospinning nanofibers as uniaxially aligned arrays and layer-by-layer stacked films. Adv Mater 2004;16(4):361–6.
[10] Dong H, Bell T. State-of-the-art overview: ion beam surface modification of polymers towards improving tribological properties. Surf Coat Technol 1999;111(1):29–40.
[11] Guenther M, Sahre K, Suchaneck G, Gerlach G, Eichhorn KJ. Influence of ion-beam induced chemical and structural modification in polymers on moisture uptake. Surf Coat Technol 2001;142–144: 482–8.
[12] Turos A, Jagielski J, Piatkowska A, Bielinski D, Slusarski L, Madi NK. Ion beam modification of surface properties of polyethylene. Vacuum 2003;70(2–3):201–6.
[13] Wong KH, Zinke-Allmang M, Wan WK, Zhang JZ, Hu P. Low energy oxygen ion beam modification of the surface morphology and chemical structure of polyurethane fibers. Nucl Inst Methods Phys Res B 2006;243(1):63–74.
[14] Calcagno L. Ion-chains interaction in polymers. Nucl Inst Methods Phys Res B Beam Interact Mater Atoms 1995;105(1–4):63–70.
[15] Wong KKH, Zinke-Allmang M, Wan WK. N+ surface doping on nanoscale polymer fabrics via ion implantation. Nucl Inst Methods Phys Res B Beam Interact Mater Atoms 2006;249(1–2):362–5.
[16] Rodríguez RJ, García JA, Sánchez R, Pérez A, Garrido B, Morante J. Modification of surface mechanical properties of polycarbonate by ion implantation. Surf Coat Technol 2002;158–159:636–42.
[17] Pivin JC. Contribution of ionizations and atomic displacements to the hardening of ion-irradiated polymers. Thin Solid Films 1995;263(2): 185–93.
[18] Rhee KY, Oh TY, Paik YN, Park HJ, Kim SS. Tensile behavior of polyethylene fiber composites with polyethylene fiber surface-modified using ion irradiation. J Mater Sci 2004;39(5):1809–11.
[19] Pelham RJ, Wang Yl. Cell locomotion and focal adhesions are regulated by substrate flexibility. Proc Natl Acad Sci USA 1997;94(25):13661–5.
[20] Discher DE, Janmey P, Wang Yl. Tissue cells feel and respond to the stiffness of their substrate. Science 2005;310:1139–43.
[21] Kusakabe M, Suzuki Y, Nakao A, Kaibara M, Iwaki M, Scholl M. Control of endothelial cell adhesion to polymer surface by ion implantation. Polym Adv Technol 2001;12(8):453–60.
[22] Bullett NA, Bullett DP, Truica-Marasescu FE, Lerouge S, Mwale F, Wertheimer MR. Polymer surface micropatterning by plasma and VUV-photochemical modification for controlled cell culture. Appl Surf Sci 2004;235(4):395–405.
[23] Girard-Lauriault PL, Mwale F, Iordanova M, Demers C, Desjardins P, Wertheimer MR. Atmospheric pressure deposition of micropatterned nitrogen-rich plasma-polymer films for tissue engineering. Plasma Process Polym 2005;2(3):263–70.
[24] DeMerlis CC, Schoneker DR. Review of the oral toxicity of polyvinyl alcohol (PVA). Food Chem Toxicol 2003;41(3):319–26.
[25] Guhados G, Wan WK, Hutter JL. Measurement of the elastic modulus of single bacterial cellulose fiber using atomic force microscopy. Langmuir 2005;21(14):6642–6.
[26] Ziegler JF, Biersack JP, Littmark U. The stopping and range of ions in solids. New York: Pergamon; 1985.
[27] Press WH, Teukolsky SA. Numerical recipes in C: the art of scientific computing. Cambridge, UK: Cambridge University Press; 1992.
[28] Hutter JL, Bechhoefer J. Calibration of atomic-force microscope tips. Rev Sci Instrum 1993;64(7):1868–73.
[29] Yang L, Fitié CFC, van der Werf KO, Bennink ML, Dijkstra PJ, Feijen J. Mechanical properties of single electrospun collagen type I fibers. Biomaterials 2008;29(8):955–62.
[30] Gu SY, Wu QL, Ren J, Vancso GJ. Mechanical properties of a single electrospun fiber and its structures. Macromol Rapid Commun 2005;26(9):716–20.
[31] Timoshenko S, Gere JM. Mechanics of materials. 4th ed. Boston, MA: PWS Publishing Co.; 1996.
[32] Press WH, Teukosky SA, Vetterling WT, Flannery BP. Numerical recipes in Fortran77. Cambridge, UK: Cambridge University Press; 1986.
[33] Koski A, Yim K, Shivkumar S. Effect of molecular weight on fibrous PVA produced by electrospinning. Mater Lett 2004;58(3–4):493–7.
[34] Mit-uppatham C, Nithitanakul M, Supaphol P. Ultrafine electrospun polyamide-6 fibers: effect of solution conditions on morphology and average fiber diameter. Macromol Chem Phys 2004;205(17): 2327–38.
[35] Tripatanasuwan S, Zhong Z, Reneker DH. Effect of evaporation and solidification of the charged jet in electrospinning of poly(ethylene oxide) aqueous solution. Polymer 2007;48(19):5742–6.
[36] Yu YC, Hsu JY, Liang JH, Chen KM. Energy loss straggling of energetic 3He and 6Li ions into polymer foils. Nucl Inst Methods Phys Res B 2006;249(1–2):47–50.
[37] Findlay DM, Welldon K, Atkins GJ, Howie DW, Zannettino ACW, Bobyn D. The proliferation and phenotypic expression of human osteoblasts on tantalum metal. Biomaterials 2004;25(12): 2215–27.
[38] Levine BR, Sporer S, Poggie RA, Della Valle CJ, Jacobs JJ. Experimental and clinical performance of porous tantalum in orthopedic surgery. Biomaterials 2006;27(27):4671–81.
[39] Yu SB, Watson AD. Metal-based X-ray contrast media. Chem Rev 1999;99(9):2353–78.
[40] de Souza JP, Suprun-Belevich Y, Boudinov H, Cima CA. Mechanical strain and damage in Si implanted with O and N ions at elevated temperatures: evidence of ion beam induced annealing. J Appl Phys 2001;89(1):42–6.
[41] Ohl A, Schröder K. Plasma-induced chemical micropatterning for cell culturing applications: a brief review. Surf Coat Technol 1999;116–119:820–30.
[42] Wagner AJ, Fairbrother DH, Reniers F. A comparison of PE surfaces modified by plasma generated neutral nitrogen species and nitrogen ions. Plasmas Polym 2003;8(2):119–34.
[43] Upadhyay DJ, Bhat NV. Pervaporation studies of gaseous plasma treated PVA membrane. J Membr Sci 2004;239(2):255–63.
[44] Shin MK, Kim SI, Kim SJ, Kim SK, Lee H, Spinks GM. Size-dependent elastic modulus of single electroactive polymer nanofibers. Appl Phys Lett 2006;89:231929.
[45] Arinstein A, Burman M, Gendelman O, Zussman E. Effect of supramolecular structure on polymer nanofibre elasticity. Nat Nanotechnol 2007;2:59–62.
[46] Beamson G, Briggs D. High resolution XPS of organic polymers. John Wiley & Son Ltd.; 1992.
[47] Chapiro A. Radiation chemistry of polymeric systems. New York: Interscience Publishers; 1962.
[48] Yokota T, Terai T, Kobayashi T, Iwaki M. Cell adhesion to nitrogen-doped DLCS fabricated by plasma-based ion implantation and deposition method. Nucl Inst Methods Phys Res B 2006;242(1–2): 48–50.